Effects of residual hydrogen in sputtering atmosphere on structures and properties of amorphous In-Ga-Zn-O thin films

Haochun Tang, Kyohei Ishikawa, Keisuke Ide, Hidenori Hiramatsu, Shigenori Ueda, Naoki Ohashi, Hideya Kumomi, Hideo Hosono, and Toshio Kamiya'

Citation: Journal of Applied Physics **118**, 205703 (2015); doi: 10.1063/1.4936552
View online: http://dx.doi.org/10.1063/1.4936552
View Table of Contents: http://aip.scitation.org/toc/jap/118/20
Published by the American Institute of Physics

Effects of residual hydrogen in sputtering atmosphere on structures and properties of amorphous In-Ga-Zn-O thin films

Haochun Tang,[1] Kyohei Ishikawa,[1] Keisuke Ide,[1] Hidenori Hiramatsu,[1,2] Shigenori Ueda,[3] Naoki Ohashi,[2,3] Hideya Kumomi,[2] Hideo Hosono,[1,2] and Toshio Kamiya[1,2,a)]
[1]*Materials and Structures Laboratory, Tokyo Institute of Technology, 4259 Nagatsuta, Midori-ku, Yokohama 226-8503, Japan*
[2]*Materials Research Center for Element Strategy, Tokyo Institute of Technology, 4259 Nagatsuta, Midori-ku, Yokohama 226-8503, Japan*
[3]*National Institute for Materials Science, 1-2-1 Sengen, Tsukuba-city, Ibaraki 305-0047, Japan*

(Received 29 September 2015; accepted 13 November 2015; published online 30 November 2015)

We investigated the effects of residual hydrogen in sputtering atmosphere on subgap states and carrier transport in amorphous In-Ga-Zn-O (a-IGZO) using two sputtering systems with different base pressures of $\sim 10^{-4}$ and 10^{-7} Pa (standard (STD) and ultrahigh vacuum (UHV) sputtering, respectively), which produce a-IGZO films with impurity hydrogen contents at the orders of 10^{20} and 10^{19} cm^{-3}, respectively. Several subgap states were observed by hard X-ray photoemission spectroscopy, i.e., peak-shape near-valence band maximum (near-VBM) states, shoulder-shape near-VBM states, peak-shape near-conduction band minimum (near-CBM) states, and step-wise near-CBM states. It was confirmed that the formation of these subgap states were affected strongly by the residual hydrogen (possibly H_2O). The step-wise near-CBM states were observed only in the STD films deposited without O_2 gas flow and attributed to metallic In. Such step-wise near-CBM state was not detected in the other films including the UHV films even deposited without O_2 flow, substantiating that the metallic In is segregated by the strong reduction effect of the hydrogen/H_2O. Similarly, the density of the near-VBM states was very high for the STD films deposited without O_2. These films had low film density and are consistent with a model that voids in the amorphous structure form a part of the near-VBM states. On the other hand, the UHV films had high film densities and much less near-VBM states, keeping the possibility that some of the near-VBM states, in particular, of the peak-shape ones, originate from –OH and weakly bonded oxygen. These results indicate that 2% of excess O_2 flow is required for the STD sputtering to compensate the effects of the residual hydrogen/H_2O. The high-density near-VBM states and the metallic In segregation deteriorated the electron mobility to 0.4 cm^2/(V s). © *2015 AIP Publishing LLC*.
[http://dx.doi.org/10.1063/1.4936552]

I. INTRODUCTION

Amorphous oxide semiconductors (AOSs) represented by amorphous In-Ga-Zn-O (a-IGZO) are promising materials for channel layers in thin-film transistors (TFTs) due to their large electron mobilities (>10 cm^2/(V s)), small subthreshold voltage swing (<0.2 V decade^{-1}), and low temperature fabrication process.[1,2] Therefore, a-IGZO TFTs have attracted much attention and actually employed in high-resolution and/or high-frame rate active-matrix liquid-crystal displays and organic light-emitting diode displays.[3–5]

It is known that conventional amorphous semiconductors such as hydrogenated amorphous silicon (a-Si:H) have localized tail states and subgap density of states (DOSs) originating from their disordered structures and defects, which strongly affect the carrier transport properties and often cause serious deteriorations of device performances.[6] Similar to a-Si:H, a-IGZO has tail states and shallow electron traps, but their densities are 2–3 orders of magnitude lower than those of a-Si:H.[7] On the other hand, a-IGZO has high-density subgap defects in a very deep energy region just above the valence band maximum (near-VBM states) and some films exhibit signal peaks from the Fermi energy (E_F) (near-conduction band minimum (CBM) states)[8,9] as observed by photoemission spectroscopy. In these several years, near-VBM states have gathered much attention because they are recognized to be associated with the instability issues of TFTs, in particular against light-illumination stress by subgap photons.[10–13] Hard X-ray photoemission spectroscopy (HAXPES), which employs high-energy X-ray ($h\nu$ = e.g., 6–8 keV) from synchrotron energy source, is useful to observe these subgap defects and provides much reliable information from a deep bulk region due to its large escape-depth (δ_0) of photoelectron (e.g., $\delta_0 = 5.8$ nm for a-IGZO with $h\nu = 7940$ eV).[9,14] Since the report of the near-VBM states in a-IGZO by HAXPES, many groups[15–17] have investigated the origins of the near-VBM states. Our group firstly indicated that oxygen deficiencies with free space (voids) would be a plausible origin based on density functional theory (DFT) calculation;[18,19] while, weakly bonded (in other words, undercoordinated or disordered) O is also considered as another origin based on experimental results[20] and beyond-DFT calculations.[15,16,21,22]

a)Author to whom correspondence should be addressed. Electronic mail: kamiya.t.aa@m.titech.ac.jp

On the other hand, some groups including us have reported that the usual a-IGZO films contain impurity hydrogen at concentrations [H] > 10^{20} cm^{-3},[17,23–26] and the impurity hydrogen exists as the form of –OH. The [H] values in the films are reduced effectively to [H] > 10^{19} cm^{-3} by employing a much cleaner deposition chamber and/or introducing higher purity Ar and O_2 gases.[25,27] The impurity hydrogen causes many different effects; some hydrogen atoms passivate shallow traps and improved TFT performance,[24] while some ones cause extra threshold voltage (V_{th}) shift (ΔV_{th})[28] and temperature instability.[29] Therefore, it is proposed that the impurity hydrogen atoms in a-IGZO work as shallow donors, but the generated free electrons are trapped and compensated by excess oxygen atoms/molecules incorporated during the film deposition and/or thermal annealing.[30–32] Moreover, –OH is also an origin for the near-VBM states as confirmed in Ref. 30. Recently, Sallis *et al.* reported an unusual subgap feature in a-IGZO films sputtered without O_2 supply, and detected the segregated metallic In in their a-IGZO films by 4 keV HAXPES.[33]

In this work, we will show that the above results such as In segregation and the density of the near-VBM states are affected largely by the base pressure (P_{base}) of the deposition chamber and thus by the amount of the residual hydrogen in the sputtering atmosphere. We employed two sputtering systems with different P_{base} (10^{-4} and 10^{-7} Pa, respectively) to investigate the effects of residual hydrogen on subgap states in a-IGZO. We found that the film structure (i.e., the film density) and subgap defects depend largely on P_{base}, in particular when films were deposited without O_2 supply. For example, the impurity hydrogen caused a strong reduction reaction in the poor P_{base} sputtering process to segregate metallic In as reported in Ref. 33, while such In segregation was not detected for the good P_{base} films. Similarly, the poor P_{base} films exhibited much higher density of the near-VBM states than the good P_{base} films. The poor P_{base} films exhibited low film density, suggesting that oxygen deficient atmosphere forms much defective (i.e., with voids) structure in a-IGZO; while, thermal desorption spectra suggest that some of the near-VBM states originate from –OH and weakly bonded O.

II. EXPERIMENT

A-IGZO films were grown at room temperature (RT) using a polycrystalline $InGaZnO_4$ target with two radio-frequency magnetron sputtering (RFMS) systems with different P_{base}; one is a conventional (standard, STD) RFMS with usual $P_{base} \sim 10^{-4}$ Pa, and the other is ultrahigh vacuum (UHV) RFMS with $P_{base} \sim 10^{-7}$ Pa. The hydrogen content in the resulted films is at the orders of 10^{20} and 10^{19} cm^{-3}, respectively, for the poor and good P_{base} RFMS.[25] Ar and O_2 mixing gases were flown during the sputtering deposition with the fixed total gas flow rate of 20 sccm and the fixed total pressure of 0.55 Pa. The RF power of the STD sputtering was 70 W and that of the UHV sputtering was 100 W, which were chosen from our previous studies. The oxygen flow rate ratio $R_{O2} = [O_2]/([O_2]+[Ar])$ was varied from 0% to 5% for STD and from 0% to 1% for UHV because we have confirmed that the optimum R_{O2} were ~3% for STD and <1% for UHV sputtering.

Optical transmittance (T) and reflectance (R) spectra were measured with an ultraviolet–visible–near-infrared spectrophotometer, and the absorption coefficient (α) spectra were obtained using the reflection correction equation $\exp(-\alpha d) = T/(1-R)$ (d is the film thickness).[34,35] The grazing-incidence X-ray reflectivity spectroscopy (XRR) was employed to evaluate the film density by fitting with a three layers model composed of surface a-IGZO layer with surface roughness/bulk a-IGZO layer/glass substrate. The chemical compositions were measured by X-ray fluorescence spectroscopy (XRF). HAXPES measurements were performed at the BL15XU undulator beamline (excitation X-ray energy: $h\nu = 5950.3$ eV) in SPring-8.[36] Electrical properties including conductivity (σ), Hall mobility (μ_{Hall}), and carrier concentration (N_e) were obtained by Hall effect measurements using the van der Pauw configuration at RT. Thermal desorption spectroscopy (TDS) was employed to investigate the gas desorption behaviors (H_2, O_2, H_2O, and Ar).

III. RESULTS

Figure 1(a) shows the α spectra of the STD a-IGZO films deposited at various R_{O2} = 0%–5%. It is seen that the R_{O2} = 0% film has a long tail subgap absorption extending from the optical band gap ($E_g \sim 3.0$ eV, determined by Tauc' plot) at least down to the near-infrared region 0.5 eV. The subgap absorption intensity is reduced significantly when R_{O2} was increased only to 1% and almost eliminated at R_{O2} = 3% (note that this is the optimum condition to produce good a-IGZO TFTs without post-fabrication thermal annealing[20,37]). Unlike the STD films, the UHV film deposited at R_{O2} = 0% showed much weaker subgap absorption resembling to the STD R_{O2} = 1% film (Fig. 1(b)). Very slight addition of oxygen at R_{O2} = 0.1% was enough to eliminate the subgap absorption in the UHV film, whose α spectrum is similar to those of the STD 3% and 5% films.

HAXPES spectra show several subgap states as seen in Figs. 2(a) and 2(b), i.e., peak-shape near-VBM states (See the energy region from the VBM energy (E_{VBM}) to 1.5 eV for the R_{O2} = 0% in Fig. 2(a). Weak but similar features are detected also in the other STD films.), shoulder-shape near-VBM states (see the UHV films in Fig. 2(b)), peak-shape

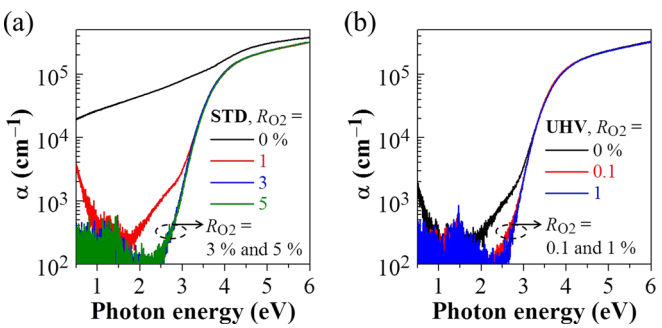

FIG. 1. Optical absorption (α) spectra of films deposited by (a) STD and (b) UHV sputtering with various R_{O2}. The STD R_{O2} = 0% film shows a long tail subgap absorption from E_g at least to 0.5 eV, while such strong subgap absorption was not observed in the UHV R_{O2} = 0% film.

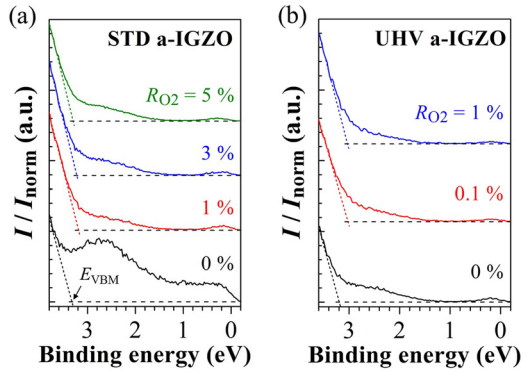

FIG. 2. HAXPES spectra around the band gap region for (a) STD and (b) UHV a-IGZO as a function of R_{O2}. The VBM energies (E_{VBM}) are shown by the cross sections of the dashed straight lines in the figures.

near-CBM states (all the films except for the STD $R_{O2} = 0\%$ film), and step-wise near-CBM states (the STD $R_{O2} = 0\%$ film). As already reported, a-IGZO films have high-density occupied defect states extending from E_{VBM} to ~1.5 eV toward E_F.[8] In particular, the STD $R_{O2} = 0\%$ film has very high-density near-VBM states with a peak-type shape. The density of the near-VBM states decreased dramatically when R_{O2} was increased only to 1% and leveled off at higher R_{O2}. On the other hand, the UHV 0% film exhibited much smaller density of the near-VBM states. These results correspond well to the small subgap absorption of the UHV 0% film in Fig. 1(b).

It is also found that the subgap states in the STD 0% film include extra near-CBM states other than the usual near-VBM states (usually appear from VBM to ~1.5 eV above VBM) because a step-wise continuous signal extends from 1.5 eV to E_F, whose shape resembles the DOS of a metal (step-wise near-CBM states). As seen in the HAXPES core spectra in Fig. 3, only the In 3d spectra of the STD 0% film show satellite peaks at 443.9 and 451.5 eV beside the main peaks at 445.3 and 452.8 eV, respectively, where the main peaks are attributed to the In^{3+} state in oxides and the satellite peaks to metallic indium (In^0),[33,38] which is consistent with the metal-like step-wise near-CBM states extending to E_F in Fig. 2(a) and the strong subgap optical absorption in Fig. 1(a). As reported in Ref. 29 by DFT, it would be reasonable to consider that oxygen deficiencies are formed preferably near In ions because of the smallest In–O bonding energy among the metal—O ones in a-IGZO, which would lead to the segregation of In^0. It should be noted that such In^0 segregation was not detected in the UHV films even deposited without O_2 supply ($R_{O2} = 0\%$). From these results, we conclude that the long tail subgap absorption in Fig. 1(a) comes from the metal-like step-wise near-CBM states in Fig. 2(a). The segregation of the In^0 and the consequent formation of the near-CBM states were already reported in Ref. 33. However, the present result shows that this In^0 segregation behavior is not inherent to a-IGZO growth but should be attributed to residual hydrogen in a sputtering atmosphere.

Different from the STD 0% films, broad peak-shape near-CBM states, which are strikingly different from the metal-like step-wise shape, are observed in all the other STD and UHV films. The peak-shape near-CBM states were

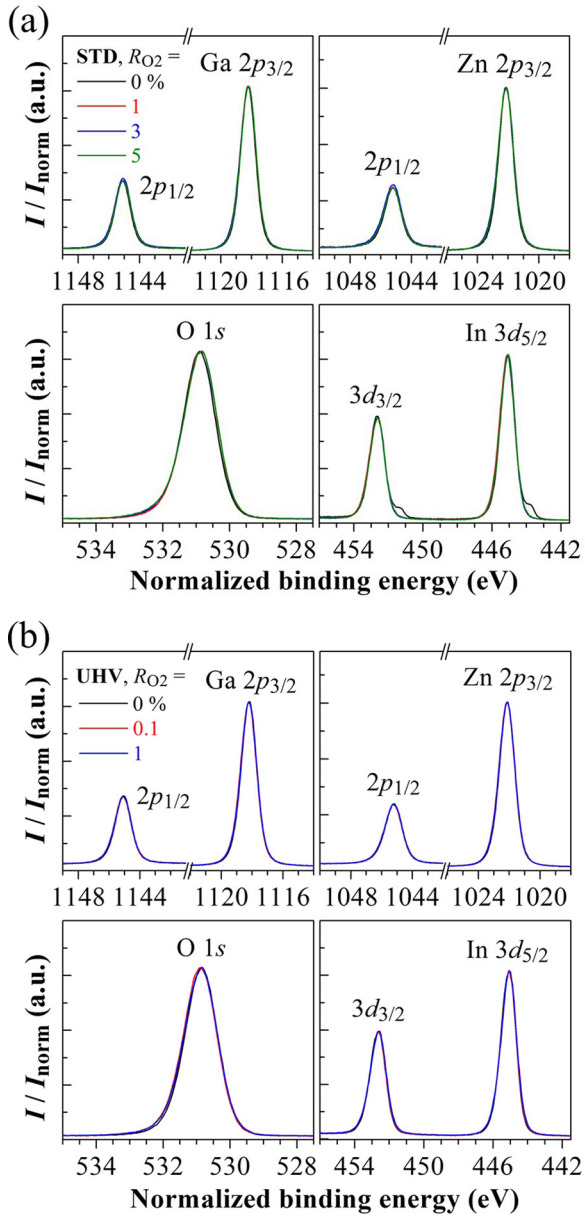

FIG. 3. HAXPES core spectra for (a) STD and (b) UHV films. The peak intensities and the peak energies are calculated by those of In 3d.

already reported[9] and observed in good a-IGZO films rather than defective films.[39] On the other hand, the STD 0% films exhibited the step-wise near-CBM states and they are similar to the HAXPES spectrum of In metal as compared in Figs. 4(a) and 4(b). Therefore, we can safely conclude that the step-wise near-CBM states are attributed to In metal. However, these still remains a possibility that the peak-shape near-CBM states observed in the other films originate also from other types of In segregations such as small In clusters. Therefore, we performed first-principles DFT calculations using a VASP code.[40] Figure 4(c) compares the DOSs calculated for In clusters with various diameters ($D = 0.7$ nm for In_6 cluster and 1.2 nm for In_{43} cluster), that of bulk In metal, and the HAXPES spectrum of the STD 3% film with the peak-shape near-CBM states. We can see that the In_{43} cluster and larger models including bulk In have rather flat DOSs while the near-CBM states of the STD 3% film have a peak

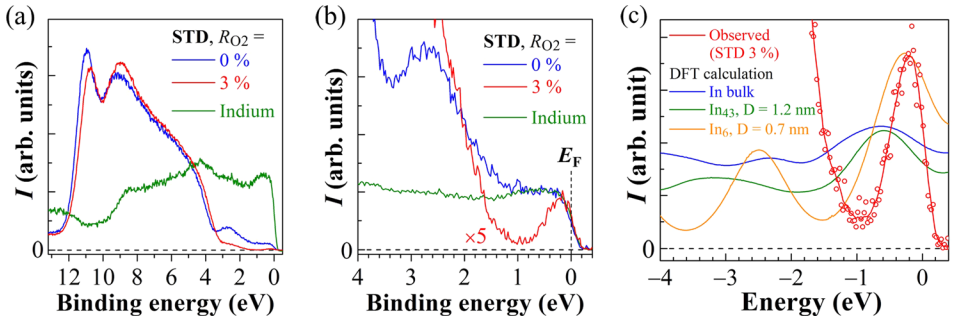

FIG. 4. (a) Valence band spectra for STD films along with In metal. (b) Expanded view of (a). The intensities are normalized around the E_F. (c) DOS of In clusters calculated by DFT. For comparison, an expanded spectrum of the STD 3% film in (b) is superimposed.

shape with a clear valley at ~−1.0 eV. Although the very small In_6 cluster has a peak shape similar to the observed near-CBM states, but the peak width of its DOS is almost double of that of the observed near-CBM states. Therefore, we exclude the In cluster segregation from a possible origin of the peak-shape near-CBM state.

Here, we like to discuss origins of the near-VBM states. Although the STD 0% film had the very high-density near-VBM states as seen in Fig. 2(a), the density of the near-VBM states in the UHV 0% film was much lower. They were reduced significantly when appropriate amounts of O_2 gas were supplied for the sputtering deposition. To examine the possibility of voids as an origin of near-VBM states, film densities were measured by XRR as shown in Fig. 5. Figure 5(a) shows an example of XRR spectrum for the STD 3% a-IGZO film with the thickness of ~40 nm. It is seen that the three layers model provided good fitting results, guaranteeing the reliability of the obtained parameters such as the film density, thickness, and surface roughness. Figure 5(b) shows the XRR spectra magnified in the vicinity of the critical angles of the STD and the UHV films as a function of R_{O2}, which shows that the density of the STD a-IGZO films decreases with decreasing R_{O2}, while that of the UHV a-IGZO films almost unchanged as summarized in Fig. 5(c). It should be noted that only the STD film deposited without O_2 (i.e., $R_{O2} = 0\%$) has the very low density $\rho = 5.93\ g/cm^3$, which is much smaller than those of the STD films deposited with O_2 (i.e., $R_{O2} \geq 1\%$) and those of the UHV films. It indicates that the STD 0% film is much defective with voids (probably nanometer size or less), which would reasonably be attributed to oxygen deficiency.

On the other hand, the UHV film shows a larger density $\rho = 6.12\ g/cm^3$ than that of the STD 0% film even if deposited without O_2 (i.e., $R_{O2} = 0\%$). The ρ value of the UHV film is reduced slightly to $6.08\ g/cm^3$ at $R_{O2} = 0.1\%$ or higher, which is attributed to the chemical composition change as observed by XRF in Fig. 6. Figure 6(a) shows the XRF core spectra of Ga Kα and Zn Kα normalized by corresponding In Kα spectra (i.e., the peak intensities in Fig. 6(a) correspond to the Ga/In and the Zn/In ratios) for the STD and the UHV a-IGZO films, which are summarized in Fig. 6(b) (the peak area ratios were converted to the atomic ratios by the calibration procedure reported in Ref. 25). As reported in this reference, the UHV a-IGZO films had almost stoichiometric compositions of In:Ga:Zn = 1:1.03:1.06 when R_{O2} is 0.1% or larger, while the Zn and Ga contents were reduced slightly to In:Ga:Zn = 1:0.95:0.91 when R_{O2} is 0%, which would explain the larger ρ of the UHV 0% film than that of the UHV 0.1%–1% films as observed in Fig. 5(b) because the molecular weight is larger for the In-rich compositions. On the other hand, all the STD films have lower Zn contents with [Zn]/[In] ≈ 0.6, which is consistent with our previous report.[25]

IV. DISCUSSION

To explain the different behaviors between the STD and the UHV a-IGZO films, first we considered the effects of residual hydrogen in the sputtering chamber. As seen in the α spectra (Fig. 1) and HAXPES spectra (Fig. 2), the R_{O2} values required to attain the small subgap states is much larger for the STD films ($R_{O2} \geq 1\%$) than that for the UHV films ($R_{O2} \geq 0.1\%$). Moreover, the very high-density near-VBM states and the step-wise near-CBM states originating from the In^0 segregation were detected only in the STD 0% film, suggesting that residual hydrogen causes the strong reduction reaction during deposition, leading to the formation of these defects.

As for the origin of the near-VBM states, we reported that the near-VBM states come not only from the voids and weakly bonded O but also from –OH.[30] In the case of the STD 0% film, we observed the large reduction of the film density, and it is consistent with a model that voids would be an origin of the near-VBM states. On the other hand, since the higher-density near-VBM states were observed in the STD films, there remains possibility that impurity hydrogen

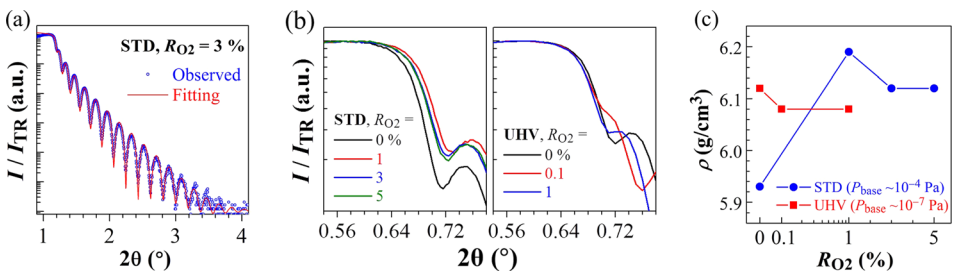

FIG. 5. XRR spectra. (a) An example of XRR full spectra for the STD 3% a-IGZO film with raw data and fitting result. (b) XRR spectra in the vicinity of critical angles of the STD and the UHV films with various R_{O2}. (c) Film densities of the STD and the UHV a-IGZO films as a function of R_{O2}.

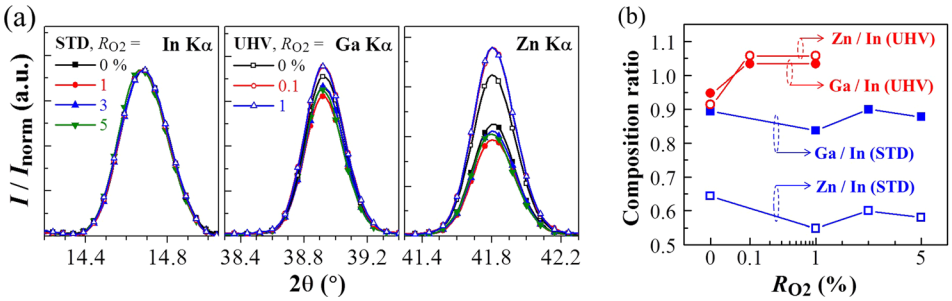

FIG. 6. Chemical composition analysis results by XRF. (a) XRF spectra normalized by the intensities of In Kα peaks. (b) Chemical composition ratios Zn/In and Ga/In as a function of R_{O2}.

forms a part of the near-VBM states. To figure out the chemical bonding states of impurity hydrogen, we performed TDS measurements. Figure 7 shows the TDS spectra of desorption gases such as H_2, O_2, H_2O, and Ar for the STD and the UHV a-IGZO films. First, we should note that the H_2, O_2, and H_2O desorption are negligible for all the UHV films while those from the STD films are very high in particular, for H_2O. It is thought that the residual gas in vacuum chamber evacuated with a turbo molecular pump (i.e., not a cryopump neither a getter pump) would contain H_2O, H_2, etc., and the chemical species generated in plasma may be H, H_2, OH, H_2O, and related ions/excited species. This TDS result implies that the major species to affect the film growth would be H_2O and OH rather than H and H_2. It is seen that large amounts of H_2O were desorbed at $T_{desorp} = 200$–$400\,^{\circ}C$ for the STD 0% films. Although the other STD films also showed H_2O desorption, but their T_{desorp} are much higher, 300–600 °C. Similarly, O_2 desorption was also detected for all the STD films, but T_{desorp} of the STD 0% film is much lower (200–400 °C) than those of the other STD films (300–600 °C). On the other hand, all the UHV films did not exhibit detectable desorption of H_2, O_2, and H_2O (note that the H_2O desorption at $T_{desorp} \leq 200\,^{\circ}C$ should be attributed to physical adsorption). These results indicate that the impurity hydrogen incorporated from the residual gas in the sputtering chamber (i.e., for the STD films) produces weakly bonded O, H, and –OH. These results are consistent with our previous reports[25] and follow the model that the impurity hydrogen in a-IGZO films mostly exists as the form of –OH

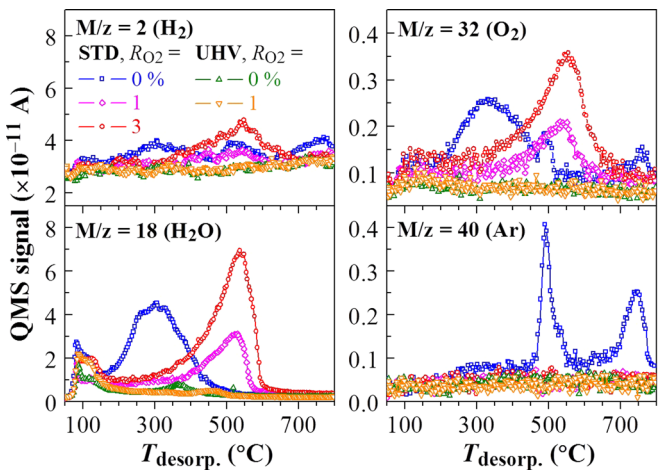

FIG. 7. TDS spectra of H_2, H_2O, O_2, and Ar for STD and UHV a-IGZO films as a function of R_{O2}.

and desorb as H_2O molecules at high temperatures. Further, sputtering without O_2 supply further weakens their chemical bonds; in other words, the STD 0% film includes very weak chemical bonds. Therefore, the possibility that weakly bonded O and H form a part of the near-VBM states is not excluded.

Next, we like to note about an origin of the low ρ of the STD 0% film. It would be natural to consider that void structures are formed in the amorphous structures and cause the low film density. However, it would also be hard to imagine that large voids are maintained in films without any inclusion atom/ion; therefore, here we like to discuss possibility of inclusion of some atoms in voids. The Ar TDS spectra in Fig. 7 show a large amount of Ar desorption only in the STD 0% film, suggesting that Ar atoms are included during the film deposition without O_2 in a poor P_{base} deposition chamber. However, occupation of an Ar atom instead of an O ion should increase the ρ because Ar has the larger atom mass of $M_{Ar} = 40$ than that of O ($M_O = 16$). On the other hand, if an Ar occupies a metal ion site (*cf.* $M_{Zn} = 65.4$, $M_{Ga} = 69.7$, $M_{In} = 114.8$), the inclusion of Ar can be a possible origin of the low ρ. Other possibilities such as inclusion of light atoms/ions such as weakly bonded O, O_2, H^0, and H^- would also be considered.

At last, we investigated the effects of the subgap states on the electron transport. Table I summarizes electrical conductivity σ, electron density N_e, and electron mobility μ_{Hall} measured by Hall effect measurements for the STD and the UHV films. Both the STD 0% film and the UHV 0% film have similar high $N_e \sim 10^{19}\,cm^{-3}$, but only the STD 0% film exhibited very low $\mu_{Hall} \sim 0.41\,cm^2/(V\,s)$ while the other films have reasonable $\mu_{Hall} = 5$–$12\,cm^2/(V\,s)$. This deterioration in the electron mobility should be related to the very high-density near-VBM states and the In^0 segregation. Since the near-VBM states are fully occupied and would be charge neutral, and are very deep from E_F, we consider that their scattering effect is not so large; therefore, the mobility

TABLE I. Transport properties (σ, N_e, and μ_{Hall}) of STD ($R_{O2} = 0\%$ and 3%) and UHV ($R_{O2} = 0\%$ and 1%) a-IGZO films.

P_{base}	R_{O2}	σ (S cm^{-1})	N_e (cm^{-3})	μ_{Hall} (cm^2/(V s))
STD (~10^{-4} Pa)	0%	4.78	7.32×10^{19}	0.41
	3%	2.48×10^{-4}	2.79×10^{14}	5.55
UHV (~10^{-7} Pa)	0%	2.69×10^{1}	1.43×10^{19}	11.8
	1%	7.41×10^{-8}	5.93×10^{12}	5.13

deterioration would be caused by locally inhomogeneous structures altered by these defects.

V. CONCLUSION

We investigated the effects of residual hydrogen in sputtering deposition on subgap states and electron transport in a-IGZO films by employing two sputtering systems with different P_{base}. The residual hydrogen/H_2O causes the strong reduction reaction which enhances the formation of the peak-shape near-VBM states and the step-wise near-CBM states. The latter is attributed to the segregation of metallic In^0, which is enhanced by the residual hydrogen/H_2O and specific to the poor P_{base} deposition system. The a-IGZO films deposited by the poor P_{base} sputtering without O_2 supply had very high-density near-VBM states, which is related to low film density (i.e., voids), impurity hydrogen (–OH), and weakly bonded O. The very high-density near-VBM states and the In^0 segregation deteriorated the electron mobility down to $\mu_{Hall} \sim 0.4\,cm^2/(V\,s)$, which would be caused by locally inhomogeneous structures altered by these defects. Decreasing the residual hydrogen/H_2O suppresses the formation of near-VBM states and the segregation of In^0 significantly even if O_2 is not supplied during sputtering deposition; in other words, 2% of excess O_2 flow is required for the poor P_{base} sputtering to compensate the reduction effects of the hydrogen.

ACKNOWLEDGMENTS

This work was supported by the Ministry of Education, Culture, Sports, Science and Technology (MEXT) through Element Strategy Initiative to Form Core Research Center. H. Hiramatsu was also supported by Support for Tokyotech Advanced Research (STAR). The HAXPES study was performed under the approval of the NIMS Synchrotron X-ray Station (Nos. 2014A4701, 2014B4702, and 2015A4704). The authors are grateful to HiSOR, Hiroshima University, and JAEA/SPring-8 for the development of the HAXPES instrumentation at BL15XU, SPring-8.

[1]K. Nomura, H. Ohta, A. Takagi, T. Kamiya, M. Hirano, and H. Hosono, Nature **432**, 488–492 (2004).
[2]T. Kamiya, K. Nomura, and H. Hosono, Sci. Technol. Adv. Mater. **11**, 044305 (2010).
[3]C. Chen, K. Abe, H. Kumomi, and J. Kanicki, J. Soc. Inf. Display **17/6**, 525–534 (2009), see http://deepblue.lib.umich.edu/bitstream/handle/2027.42/92036/JSID17.6.525.pdf?sequence=1.
[4]Y. G. Mo, M. Kim, C. K. Kang, J. H. Jeong, Y. S. Park, C. G. Choi, H. D. Kim, and S. S. Kim, J. Soc. Inf. Display **19/1**, 16–20 (2011).
[5]J. P. Lee, J. Y. Hwang, and B. S. Bae, J. Semicond. Technol. Sci. **14**, 594–600 (2014).
[6]*Technology and Application of Amorphous Silicon*, edited by R. A. Street (Springer, Berlin, 2000).
[7]M. Kimura, T. Nakanishi, K. Nomura, T. Kamiya, and H. Hosono, Appl. Phys. Lett. **92**, 133512 (2008).
[8]K. Nomura, T. Kamiya, H. Yanagi, E. Ikenaga, K. Yang, K. Kobayashi, M. Hirano, and H. Hosono, Appl. Phys. Lett. **92**, 202117 (2008).
[9]K. Nomura, T. Kamiya, E. Ikenaga, H. Yanagi, K. Kobayashi, and H. Hosono, J. Appl. Phys. **109**, 073726 (2011).
[10]K.-H. Lee, J. S. Jung, K. S. Son, J. S. Park, T. S. Kim, R. Choi, J. K. Jeong, J.-Y. Kwon, B. Koo, and S. Lee, Appl. Phys. Lett. **95**, 232106 (2009).
[11]J.-H. Shin, J.-S. Lee, C.-S. Hwang, S.-H. K. Park, W.-S. Cheong, M. Ryu, C.-W. Byun, J.-I. Lee, and H. Y. Chu, ETRI J. **31**, 62–64 (2009).
[12]K. Nomura, T. Kamiya, and H. Hosono, J. SID **18/10**, 789–795 (2010).
[13]Y. Ueoka, Y. Ishikawaz, J. P. Bermundo, H. Yamazaki, S. Urakawa, M. Fujii, M. Horita, and Y. Uraoka, ECS J. Solid State Sci. Technol. **3**(9), Q3001–Q3004 (2014).
[14]K. Kobayashi, M. Yabashi, Y. Takata, T. Tokushima, S. Shin, K. Tamasaku, D. Miwa, T. Ishikawa, H. Nohira, T. Hattori, Y. Sugita, O. Nakatsuka, A. Sakai, and S. Zaima, Appl. Phys. Lett. **83**, 1005–1007 (2003).
[15]W. Körner, D. F. Urban, and C. Elsaüsser, J. Appl. Phys. **114**, 163704 (2013).
[16]S. Sallis, K. T. Butler, N. F. Quackenbush, D. S. Williams, M. Junda, D. A. Fischer, J. C. Woicik, N. J. Podraza, B. E. White, A. Walsh, and L. F. J. Piper, Appl. Phys. Lett. **104**, 232108 (2014).
[17]M. Nakashima, M. Oota, N. Ishihara, Y. Nonaka, T. Hirohashi, M. Takahashi, S. Yamazaki, T. Obonai, Y. Hosaka, and J. Koezuka, J. Appl. Phys. **116**, 213703 (2014).
[18]T. Kamiya, K. Nomura, and H. Hosono, J. Display Technol. **5**, 468–483 (2009).
[19]T. Kamiya, K. Nomura, and H. Hosono, Phys. Status Solidi A **207**, 1698–1703 (2010).
[20]K. Ide, Y. Kikuchi, K. Nomura, M. Kimura, T. Kamiya, and H. Hosono, Appl. Phys. Lett. **99**, 093507 (2011).
[21]W. Körner, P. Gumbsch, and C. Elsässer, Phys. Rev. B **86**, 165210 (2012).
[22]W. Körner, D. F. Urban, and C. Elsässer, Phys. Status Solidi A **212**, 1476–1481 (2015).
[23]K. Nomura, T. Kamiya, and H. Hosono, ECS J. Solid State Sci. Technol. **2**, P5–P8 (2012).
[24]Y. Hanyu, K. Domen, K. Nomura, H. Hiramatsu, H. Kumomi, H. Hosono, and T. Kamiya, Appl. Phys. Lett. **103**, 202114 (2013).
[25]T. Miyase, K. Watanabe, I. Sakaguchi, N. Ohashi, K. Domen, K. Nomura, H. Hiramatsu, H. Kumomi, H. Hosono, and T. Kamiya, ECS J. Solid State Sci. Technol. **3**, Q3085–Q3090 (2014).
[26]H. Godo, D. Kawae, S. Yoshitomi, T. Sasaki, S. Ito, H. Ohara, H. Kishida, M. Takahashi, A. Miyanaga, and S. Yamazaki, Jpn. J. Appl. Phys., Part 1 **49**, 03CB04 (2010).
[27]K. Kato, Y. Shionoiri, Y. Sekine, K. Furutani, T. Hatano, T. Aoki, M. Sasaki, H. Tomatsu, J. Koyama, and S. Yamazaki, J. Appl. Phys. **51**, 021201 (2012).
[28]K. Domen, T. Miyase, K. Abe, H. Hosono, and T. Kamiya, J. Display Technol. **10**, 975–978 (2014).
[29]T. Kamiya and H. Hosono, ECS Trans. **54**, 103–113 (2013).
[30]T. Orui, J. Herms, Y. Hanyu, S. Ueda, K. Watanabe, I. Sakaguchi, N. Ohashi, H. Hiramatsu, H. Kumomi, H. Hosono, and T. Kamiya, J. Display Technol. **11**, 518–522 (2015).
[31]N. Oka, T. Aoi, R. Hayashi, H. Kumomi, and Y. Shigesato, Appl. Phys. Express **5**, 075802 (2012).
[32]T. Aoi, N. Oka, Y. Sato, R. Hayashi, H. Kumomi, and Y. Shigesato, Thin Solid Films **518**, 3004–3007 (2010).
[33]S. Sallis, N. F. Quackenbush, D. S. Williams, M. Senger, J. C. Woicik, B. E. White, and L. F. J. Piper, Phys. Status Solidi A **212**, 1471–1475 (2015).
[34]R. H. Klazes, M. H. L. M. van den Broek, J. Bezemer, and S. Radelaar, Philos. Mag., Part B **45**, 377–383 (1982).
[35]Y. Hishikawa, N. Nakamura, S. Tsuda, S. Nakano, Y. Kishi, and Y. Kuwano, Jpn. J. Appl. Phys., Part 1 **30**, 1008–1014 (1991).
[36]S. Ueda, Y. Katsuya, M. Tanaka, H. Yoshikawa, Y. Yamashita, S. Ishimaru, Y. Matsushita, and K. Kobayashi, AIP Conf. Proc. **1234**, 403–406 (2010).
[37]K. Ide, K. Nomura, H. Hiramatsu, T. Kamiya, and H. Hosono, J. Appl. Phys. **111**, 073513 (2012).
[38]B. R. Natarajan, A. H. Eltoukhy, J. E. Greene, and T. L. Barr, Thin Solid Films **69**, 217–227 (1980).
[39]K. Lee, K. Nomura, H. Yanagi, T. Kamiya, and H. Hosono, Thin Solid Films **520**, 3808–3812 (2012).
[40]G. Kresse and J. Furthmüller, Phys. Rev. B **54**, 11169–11186 (1996).